ACS Catalysis

pubs.acs.org/acscatalysis
Research Article

Valuable Compounds from Pollutants: Converting PET into Enantiopure Alanine

Elena Rosini,*[,§] Caren Battaglia,[§] Davide Miani,[§] Filippo Molinari, Federico Arrigoni, Umberto Piarulli, Gianluca Molla, and Loredano Pollegioni*

Cite This: ACS Catal. 2025, 15, 17829−17843
Read Online

ACCESS | Metrics & More | Article Recommendations | Supporting Information

ABSTRACT: The enzymatic depolymerization of single-use plastic products, primarily made from poly(ethylene terephthalate) (PET), is now a reality. Herein, we report the development of an innovative tandem system process that uses engineered enzymes and *Escherichia coli* strains to depolymerize PET and convert the resulting products into enantiomers of alanine, useful amino acids, and starting point for further valorization processes. A biosynthetic pathway has been generated, consisting of twelve enzymes derived from four different microorganisms. This pathway has been optimized using recombinant proteins and whole-cells that harbor different modules of the pathway. Specifically, the S101N/F243T-ΔLCC variant was selected to degrade PET into terephthalic acid (TPA) and ethylene glycol also at 37 °C, a temperature compatible with the *E. coli* RARE strain. A recombinant *E. coli* strain catalyzed the subsequent conversion of TPA into 2-pyrone-4,6-dicarboxylic acid, which is then transformed into pyruvate by recombinant enzymes to prevent depletion of pyruvate due to cellular catabolism. Finally, pyruvate is enzymatically aminated to enantiopure D- or L-alanine. We successfully converted postconsumer PET waste into D- and L-alanine, with an overall yield of 50 mg/170 mg PET, demonstrating that the bioconversion of selected plastics into valuable biomolecules via an eco-friendly process is feasible.

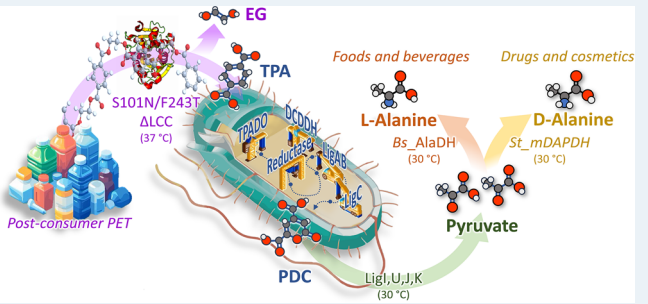

KEYWORDS: *circular bioeconomy, biotransformation, cascade reaction, plastic valorization, amino acids, system biocatalysis, engineered E. coli*

INTRODUCTION

The vast majority of plastics used today are derived from nonrenewable petrochemical feedstocks: these are recalcitrant compounds, often requiring thousands of years to biodegrade. By 2050, global plastic production is projected to exceed 33 billion tons, posing significant threats to both terrestrial and marine ecosystems as well as to human health.[1] This is primarily due to the accumulation of microplastics (plastics in the range of 1 to <1000 μm) and nanoplastics within food chains.[2] Polyethylene terephthalate (PET) poses significant challenges due to its widespread use in both large-scale distribution and domestic waste. Currently, PET is primarily treated through mechanical recycling processes or subjected to harsh chemophysical conditions (e.g., microwave radiation and temperatures up to 230 °C), resulting in a material of lower quality compared to virgin PET. Over the past decade, numerous studies have demonstrated the feasibility of biological recycling of PET, mainly through the use of engineered hydrolases. PET-hydrolyzing enzymes (PHEs) catalyze the PET depolymerization into terephthalic acid (TPA) and ethylene glycol (EG). A few efficient microbial hydrolytic enzymes capable of degrading PET to TPA have been discovered and their properties have been enhanced through protein engineering.[3−6] Recently, we developed two distinct and highly effective PHE variants: one derived from *Ideonella sakaiensis* and another from the leaf−branch compost cutinase LCC.[7,8] These extracellular enzymes achieved over 95% degradation of nanoPET and were also effective on postconsumer plastics at temperatures ≥55 °C.[9,10] TPA is known to be assimilated by bacteria and converted into protocatechuic acid (PCA) through two consecutive reactions.[11−13] PCA has been used in the biocatalytic production of various high-value compounds, including catechol, vanillin acid, vanillin, and *cis,cis*-muconic acid.[12−15]

In the context of a circular plastics economy, the conversion of waste-derived PET into valuable compounds, along with the elimination of environmental micro- and nano-PET, is of great interest. In this work, we present a novel pathway that converts TPA generated from enzymatic PET hydrolysis into PCA,

Received: September 13, 2025
Revised: October 7, 2025
Accepted: October 8, 2025
Published: October 14, 2025

Scheme 1. The novel Synthetic Pathway Converting PET into L- and D-Alanine[a]

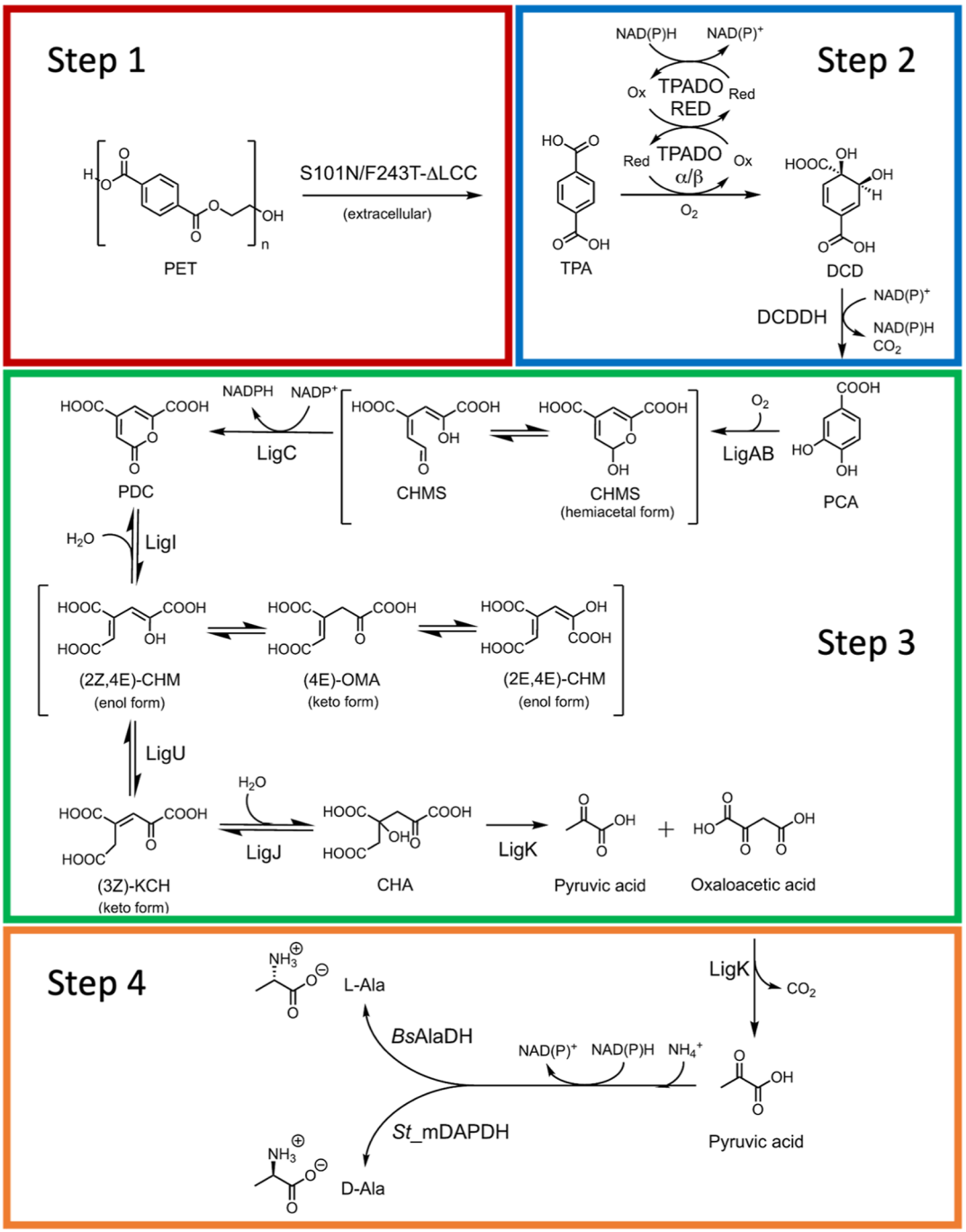

[a]The overall process has been split into four blocks. PET is depolymerized into terephthalic acid (TPA) and ethylene glycol by an engineered variant of leaf−branch compost cutinase (ΔLCC, Step 1). In Step 2, TPA is *cis*-dihydroxylated and dearomatized to produce 1,2-dihydroxy-3,5-cyclohexadiene-1,4-dicarboxylic acid (DCD) by an oxygen-dependent terephthalate dioxygenase (TPADO α/β) that works coupled to a NAD(P)H, flavin, and iron-sulfur-dependent reductase (TPADO RED). The intermediate DCD is then reductively decarboxylated yielding the key compound protocatechuic acid (PCA) by a zinc-dependent dehydrogenase (DCDDH). Step 3 starts with the cyclooxygenase LigAB: the oxygen-mediated cleavage of the aromatic ring of PCA generates the intermediate 4-carboxy-2-hydroxymuconate-6-semialdehyde (CHMS). CHMS hemiacetalic form is the substrate of LigC, an $NADP^+$-dependent enzyme which catalyzes the oxidation of the aldehydic group into a pyronic moiety to 2-pyrone-4,6-dicarboxylic acid (PDC). PDC hydrolase (LigI) cleaves the pyronic moiety of PDC into the (4*E*)-oxalmesaconate ((4*E*)-OMA) and its enolic tautomers 4-carboxy-2-hydroxymuconates ((2*Z*,4*E*)−CHM and (2*E*,4*E*)−CHM). (4*E*)-Oxalomesaconate Δ isomerase (LigU) catalyzes the isomerization of (4*E*)-OMA through an intramolecular oxidoreduction to (3*Z*)-2-keto-4-carboxy-3-hexenedioate ((3*Z*)-KCH), the preferred substrate of (4*E*)-oxalomesaconate hydratase (LigJ) which mediates the hydration of the (3*Z*)-KCH to 4-carboxy-4-hydroxy-2-oxoadipate (CHA). Finally, the CHA aldolase (LigK) generates two molecules of pyruvate through a decarboxylation reaction. Step 4 involves the reductive amination of pyruvate to yield: (a) L-Ala employing an engineered L-alanine dehydrogenase from *B. subtilis* (D196A/L197R_*Bs*AlaDH using NADPH instead of NADH as the reducing cofactor) and (b) D-Ala using the meso-diaminopimelate dehydrogenase from *Symbiobacterium thermophilum* (*St*_mDAPDH).

https://doi.org/10.1021/acscatal.5c06530
ACS Catal. 2025, 15, 17829−17843

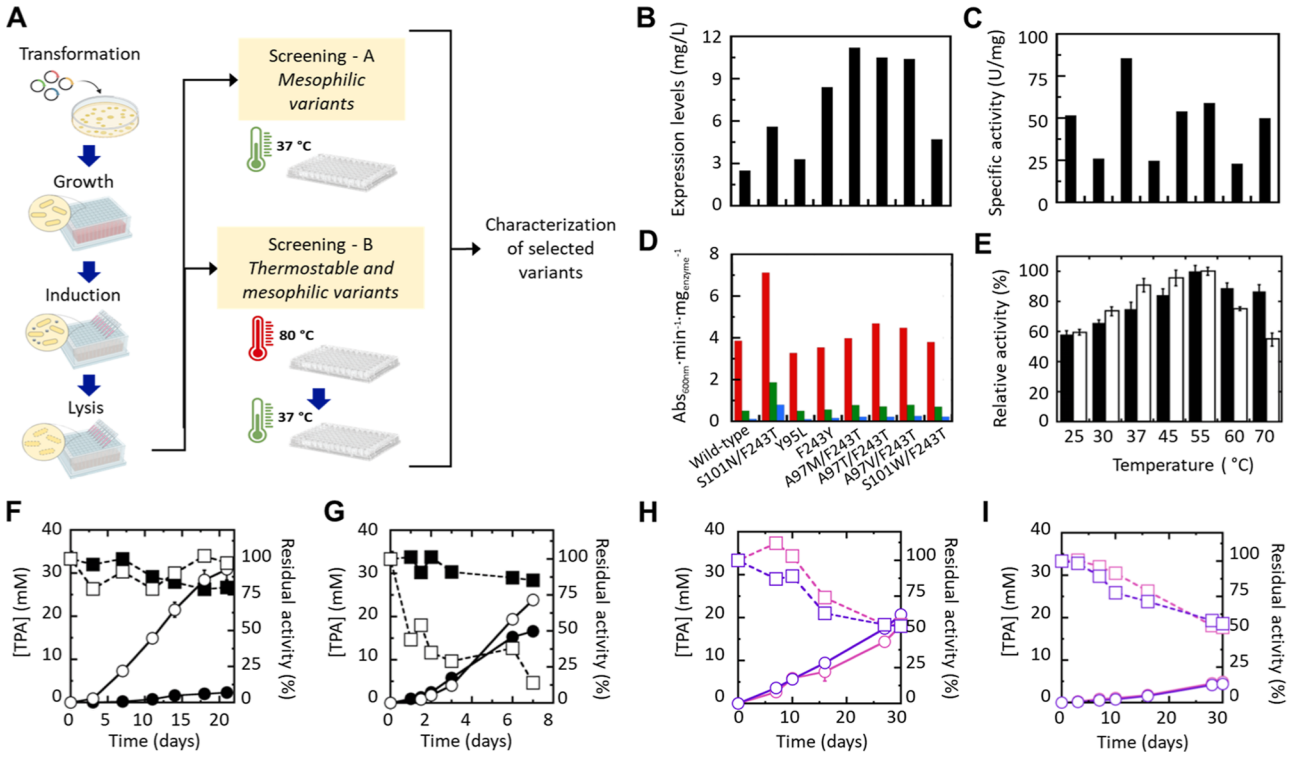

Figure 1. Evolution of a mesophilic ΔLCC variant (A–E) and PET biodegradation (F–I). (A) Scheme of the procedure used to identify ΔLCC variants active at 37 °C and stable at high temperature. (B) Expression level of the most relevant ΔLCC variants. (C) Specific activity on 1 mM *p*-NPA at 30 °C of the most relevant ΔLCC variants. (D) Activity comparison of wild-type, S101N/F243T, and six selected variants of ΔLCC on nanoPET as a substrate at three different temperatures: 30 (blue), 37 (green), and 50 °C (red). (E) Effect of temperature on the enzymatic activity of wild-type (black bars) and S101N/F243T ΔLCC (white bars), determined by measuring the hydrolytic activity on 1 mM *p*-NPA (pH 8.0). The value at 55 °C is taken as 100% (ΔLCC wild-type: 128.4 ± 3.9 U/mg; S101N/F243T ΔLCC: 67.6 ± 2.7 U/mg). (F,G) Biodegradation of 7 mg·mL^{-1} amorphous PET film by 40 μg·mL^{-1} wild-type (full symbols) or S101N/F243T-ΔLCC variant (empty symbols) in 100 mM Tris–HCl, pH 8.0 at 37 °C (F) or 55 °C (G). The TPA production (circle, continuous line) was monitored following the increase in absorbance at 240 nm of the reaction supernatant due to the accumulation of soluble aromatic products, as well as by HPLC; dashed line (square symbols) reports the residual enzymatic activity. (H,I) Biodegradation of 7 mg·mL^{-1} postconsumer PET waste samples (lid from a cheesecake container in pink and a candy tray in purple) by 40 μg·mL^{-1} S101N/F243T (H) and wild-type (I) ΔLCC in 100 mM Tris–HCl, pH 8.0 at 37 °C. Reactions were monitored as in panel F. Error bars report the standard deviation (n = 4).

which is then transformed into 2-pyrone-4,6-dicarboxylic acid (PDC). This intermediate undergoes ring cleavage through a meta-cleavage pathway, resulting in the formation of pyruvate, which is ultimately converted into D- and L-alanine (D-Ala and L-Ala) (Scheme 1). The D-Ala global market was valued at 153 million USD in 2024 and is projected to reach 219.8 million USD by 2030, growing at a CAGR of 6.2% during the forecasted period 2024 to 2030.[16] This growth is driven by an increasing demand for pharmaceuticals and personal care products. Meanwhile, the L-Ala market was valued at 146.5 million USD in 2024 and is expected to grow up to 204.4 million USD by 2030, with a compound annual growth rate (CAGR) of 5.7% from 2024 to 2030.[17] L-Ala is used in various therapeutic and beauty formulations and serves as a low-calorie sweetener in the food and beverage industry. Through enzymatic reactions, L-Ala can be further converted into other relevant natural amino acids (the market for which is growing at an annual rate of 7.8%) as well as unnatural ones.[18] With a growing global population, efforts to discover new and sustainable protein sources are more critical than ever.

L-Ala is mainly produced on an industrial scale through enzymatic conversion and microbial fermentation. The enzymatic method relies on the use of L-aspartate-α-decarboxylase to convert petroleum-derived L-aspartate into L-Ala.[19] This approach is highly efficient, reaching yields of around 90–95%; however, it is limited by its dependence on nonrenewable feedstocks. D-Ala is produced via microbial fermentation: the engineered *Corynebacterium glutamicum* DA-11 strain reached a productivity of 85 g/L.[20] Similarly, D-Ala high titers are also obtained by strains like *Escherichia coli* ALS929 and *Arthrobacter oxidans* HAP-1 but requiring longer fermentation times.[21]

Here, we report on a proof-of-concept process that demonstrates, for the first time, the ability of a tandem system based on engineered *E. coli* strains and recombinant enzymes to effectively convert postconsumer PET waste into valuable L-Ala and D-Ala. Producing either L- or D-enantiomers allows a broader range of market demands and maximizes the value derived from a single production system.

RESULTS AND DISCUSSION

Enzymatic PET Degradation at Moderate Temperature: Evolution of a Mesophilic LCC Variant. A variety of alternative natural and engineered PHEs are currently available.[22] In our previous work, we focused on two of the most widely studied PETases: *I. sakaiensis* PETase (*Is*PETase) and leaf–branch compost cutinase (LCC). LCC was selected based on its advantageous characteristics, including high stability, elevated specific activity, and ease of recombinant

https://doi.org/10.1021/acscatal.5c06530
ACS Catal. 2025, 15, 17829–17843

expression. In particular, product composition played a key role in this choice.[23,24] The primary products of PET hydrolysis by *Is*PETase are bis(2-hydroxyethyl) terephthalate (BHET) and mono(2-hydroxyethyl) terephthalate (MHET), with only minor amounts of TPA also being produced.[25] Complete breakdown of MHET into EG and TPA requires the additional activity of MHETase.[25] In contrast, LCC predominantly produces TPA and EG directly from PET,[10,23] making it more compatible with subsequent monomer valorization steps.

LCC exhibits optimal PET depolymerization activity at temperatures above 55 °C, and the kinetics of this process are well established.[10,23] However, such elevated temperatures are not compatible with the growth of *E. coli*, the host organism selected for implementing the biosynthetic pathway for amino acid production (see below). To address this limitation, we aimed to develop a mesophilic LCC variant suitable for integration into a whole-cell *E. coli* bioconversion system, as well as for coupling with downstream enzymatic valorization pathways, using the genes encoding both the wild-type and F243T-ΔLCC as templates for the generation of variant libraries.[10] Site-saturation mutagenesis (SSM) employing NNK primers was previously independently performed at positions 95, 96, 127, 166, 212, and 243.[10] These residues are positioned in loop-connecting regions which have been reported to favor the binding of the PET polymer chain in mesophilic enzymes, such as *Is*PETase, at moderate temperatures. Particularly, the Asp179-bearing loop of *Is*PETase (corresponding to Asp210 in LCC) revealed the highest backbone root mean-square fluctuation (RMSF) and it has been associated with improved PET degradation at ambient temperature compared to other cutinases.[26] To identify ΔLCC variants with significant activity on PET nanoparticles (nanoPET) at moderate temperatures while retaining substantial thermal stability, we developed a double high-throughput screening method. This procedure is based on a colorimetric assay using phenolsulfonphthalein (PSP) dye and consists of two parts: (A) an activity assay at 37 °C to identify variants with the highest activity under mesophilic conditions and (B) an activity assay at 37 °C following a 1 h treatment at 80 °C to identify variants that retain their thermal stability, see Figure 1A and Methods section.

High-throughput screening identified seven variants with improved activity at moderate temperatures following a temperature shock, compared to the wild-type ΔLCC; see details in Supporting Information and Figure S1. All the selected variants were expressed and purified by metal-chelating chromatography. The substitutions had an effect on both the volumetric yield and the specific enzymatic activity of *p*-nitrophenyl acetate (*p*-NPA), a parameter corresponding to the general hydrolytic activity. Notably, the Y95L and F243Y variants showed an expression level similar to that of the wild-type ΔLCC, while A97M/F243T, A97T/F243T, A97V/F243T, and S101W/F243T showed a significant improvement in the volumetric yield, ranging from 336% to 448% (Figure 1B). The hydrolytic activity on *p*-NPA was lower for all analyzed variants compared to the wild-type, except for the Y95L one (Figure 1C). The activity of the selected ΔLCC variants (20 $\mu g \cdot mL^{-1}$) and the wild-type (used as a reference) was further assessed on ≈94 $\mu g \cdot mL^{-1}$ nanoPET using a turbidimetric assay at three different temperatures: 30, 37, and 50 °C.[10] Among the variants, the S101N/F243T one exhibited the highest increase in activity compared to the wild-type ΔLCC, with enhancements of 368% at 37 °C and 668% at 30 °C (Figure 1D). Notably, all variants derived from the F243T library demonstrated significant improvements in activity at moderate temperatures. In detail, the S101N/F243T-ΔLCC variant showed a higher relative activity at moderate temperatures (30−45 °C) compared with the wild-type enzyme, Figure 1E.

Both the S101N/F243T-ΔLCC variant and the wild-type ΔLCC were utilized for the depolymerization of an amorphous PET film. Specifically, 40 μg of purified enzyme was added to 1 mL of 100 mM Tris−HCl, pH 8.0, containing a 7 mg amorphous PET film disk. The reaction mixture was incubated either at 55 °C, the optimal temperature for biodegradation by wild-type ΔLCC, or at 37 °C, the optimal temperature for *E. coli* growth. The S101N/F243T-ΔLCC variant was more efficient in PET depolymerization at 37 °C than the wild-type (30.9 mM TPA was released after 21 days of incubation, conversion yield of 85%, Figure 1F), while after 7 days of incubation at 55 °C, a similar PET degradation was observed (approximately 23.9 mM TPA was released using the S101N/F243T-ΔLCC variant, conversion yield of 50−70%, Figure 1G). The reaction rate at 55 °C was 2.2-fold faster compared to the one at 37 °C. Despite the slower PET degradation rate, the S101N/F243T-ΔLCC enzyme largely retained its initial activity at 37 °C after 21 days of incubation, whereas its activity was substantially lost within 1 week at 55 °C. The enhanced activity of the variant at 37 °C and the intrinsic stability of LCC positively influenced the PET degradation enabling prolonged PET depolymerization and higher cumulative yield. During the depolymerization of an amorphous PET film catalyzed by the S101N/F243T-ΔLCC variant, equimolar amounts of EG and TPA were released (Figure S2).

While wild-type ΔLCC is employed at temperatures ≥55 °C,[3,10] in this study, we assessed TPA production at 37 °C using two different transparent, untreated postconsumer PET waste samples: a candy tray and a cheesecake lid container. For each sample, 40 μg of the purified S101N/F243T-ΔLCC variant or wild-type ΔLCC was added to 1 mL of 100 mM Tris−HCl, pH 8.0, containing ≈7 mg PET, and incubated at 37 °C for up to 30 days. Both samples reached a final TPA concentration >20 mM (Figure 1H), corresponding to a >50% depolymerization yield. Under identical conditions, wild-type ΔLCC exhibited markedly lower PET degradation activity, producing less than 5 mM TPA, as shown in Figure 1I.

The evolved S101N/F243T-ΔLCC variant efficiently depolymerizes untreated postconsumer PET (Step 1, Scheme 1) under mild conditions compatible with *E. coli* growth. A scale-up experiment using 170 mg of postconsumer PET generated 13.6 mM TPA (83 mg) in 62 days (see below). Notably, a similar level of TPA production was obtained with wild-type ΔLCC only when incubated at 55 °C for approximately one month, highlighting the enhanced low-temperature activity of the S101N/F243T variant.

Finally, we investigated the potential of employing an extracellular form of LCC. Extracellular expression was achieved by introducing signal peptide sequences upstream of the *LCC* gene. Specifically, we evaluated three different signal peptides: the B1 signal peptide enhancer,[27] a modified version of the PelB signal peptide (PelB*),[28] and the native signal peptide SP_{NAT}.[10] After 24 h of cultivation—conditions under which enzyme purification from crude extracts was performed—the level of ΔLCC detected in the culture broth

https://doi.org/10.1021/acscatal.5c06530
ACS Catal. 2025, 15, 17829−17843

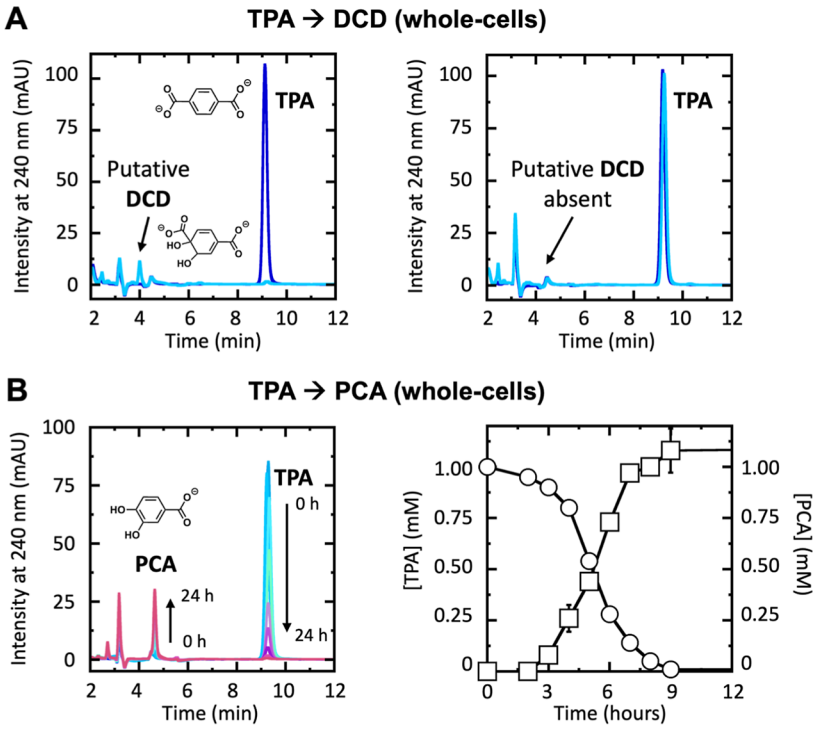

Figure 2. Enzymatic conversion of TPA into PCA at pH 7.0 in the presence of 10% glycerol. (A) HPLC analysis of whole-cell bioconversion of 1 mM TPA at 0 (blue) and after 18 h (light blue) of incubation at 30 °C using the recombinant *E. coli* strain expressing TPADO α/β and TPADO RED (left panel) or the negative control (mock, right panel). (B) Whole-cell bioconversion of 1 mM TPA into PCA by strain A. Left panel: HPLC chromatograms of samples withdrawn from the reaction mixture (from 0 to 24 h of incubation, colored from light blue to pink). Right panel: time course of TPA consumption (circles) and PCA production (squares). Error bars report the standard deviation (n = 3).

represented approximately 5% of the total expressed protein (Table S1). This proportion increased significantly over time, reaching 96% after 6 days. This result suggests that the presence of the enzyme in the culture medium may be attributed to cell lysis. Similarly, the level of B1-PelB*-ΔLCC in the culture broth also increased over time (Figure S3), accounting for 42% of the total expressed protein after 6 days. However, its overall expression was approximately 10-fold lower than that of the untagged ΔLCC. In contrast, no detectable protein expression was observed when the native SP_{NAT} signal peptide was used. Under the experimental conditions described in Figure 1H,I, the depolymerization of postconsumer PET waste using the culture broth was minimal at both 37 and 55 °C (≤1.5% after 6 days; Figure S4). These results underscore the necessity of using the purified ΔLCC enzyme to achieve efficient PET depolymerization.

Setup of the TPA Degradation Pathway. *Bioconversion of TPA into PCA.* In the in vivo enzymatic pathway for the bioconversion of TPA into PCA, TPA is initially *cis*-dihydroxylated and dearomatized by an O_2-dependent terephthalate dioxygenase (TPADO α/β) in conjunction with a NAD(P)H reductase (TPADO RED), both derived from *Comamonas* sp. strain E6.[12] The resulting intermediate 1,2-dihydroxy-3,5-cyclohexadiene-1,4-dicarboxylic acid (DCD) undergoes reductive decarboxylation by a zinc-dependent dehydrogenase (DCDDH)[12] to yield PCA, Step 2 in Scheme 1.

First, the *TPADO* α/β and *TPADO RED* encoding genes, subcloned into the medium copy number pET-Duet-1 plasmid (see Tables S2 and S3 for the list of the plasmids used and strains generated), were coexpressed in the engineered *E. coli* K-12 MG1655 RARE strain. The resulting *E. coli* K-12 MG1655 RARE pET-Duet:TPADO α/β-TPADO RED cells (100 mg cell wet weight (cww) mL^{-1}, resuspended in 100 mM Tris−HCl, pH 7.0, 10% w/v glycerol) were used for the bioconversion of 1 mM analytical-grade TPA. HPLC analysis demonstrated the complete consumption of the substrate within 18 h (Figure 2A) and the formation of a peak eluting at a retention time of 4.2 min, which was not detected when the corresponding mock *E. coli* cells were used (*E. coli* K-12 MG1655 RARE pETDuet-1): this peak was assumed to correspond to DCD, the intermediate compound of the bioconversion of TPA into PCA.

The synthetic genes encoding the full suite of enzymes required for the bioconversion of TPA to PCA (Step 2) were cloned into plasmids pETDuet-1 and pRSFDuet-1. This resulted in the generation of *E. coli* K-12 MG1655 RARE pET-Duet:TPADO α/β-TPADO RED—pRSFDuet:DCDDH (designed as strain A). As shown in Figure 2B, the coexpression of TPADO α/β, TPADO RED, and DCDDH in a single whole-cell system enabled the complete bioconversion of 1 mM TPA into PCA within 9 h. The peak assumed to correspond to the DCD reaction intermediate (see above) was no longer detected, likely due to its rapid utilization by DCDDH for PCA production. Recently, the same pathway was also utilized to upcycle PET into adipic acid using an engineered *E. coli* strain, although details about this step have not been reported.[29] Additionally, when this module was introduced in *Pseudomonas putida*, the *tpaK* gene, encoding the transporter, was also required.[30] Noteworthily, our trials did not show a need for the TPA transporter in the *E. coli* RARE strain: a similar rate of TPA consumption and PCA production was observed using strain A and strain A_tpaK,

https://doi.org/10.1021/acscatal.5c06530
ACS Catal. 2025, 15, 17829−17843

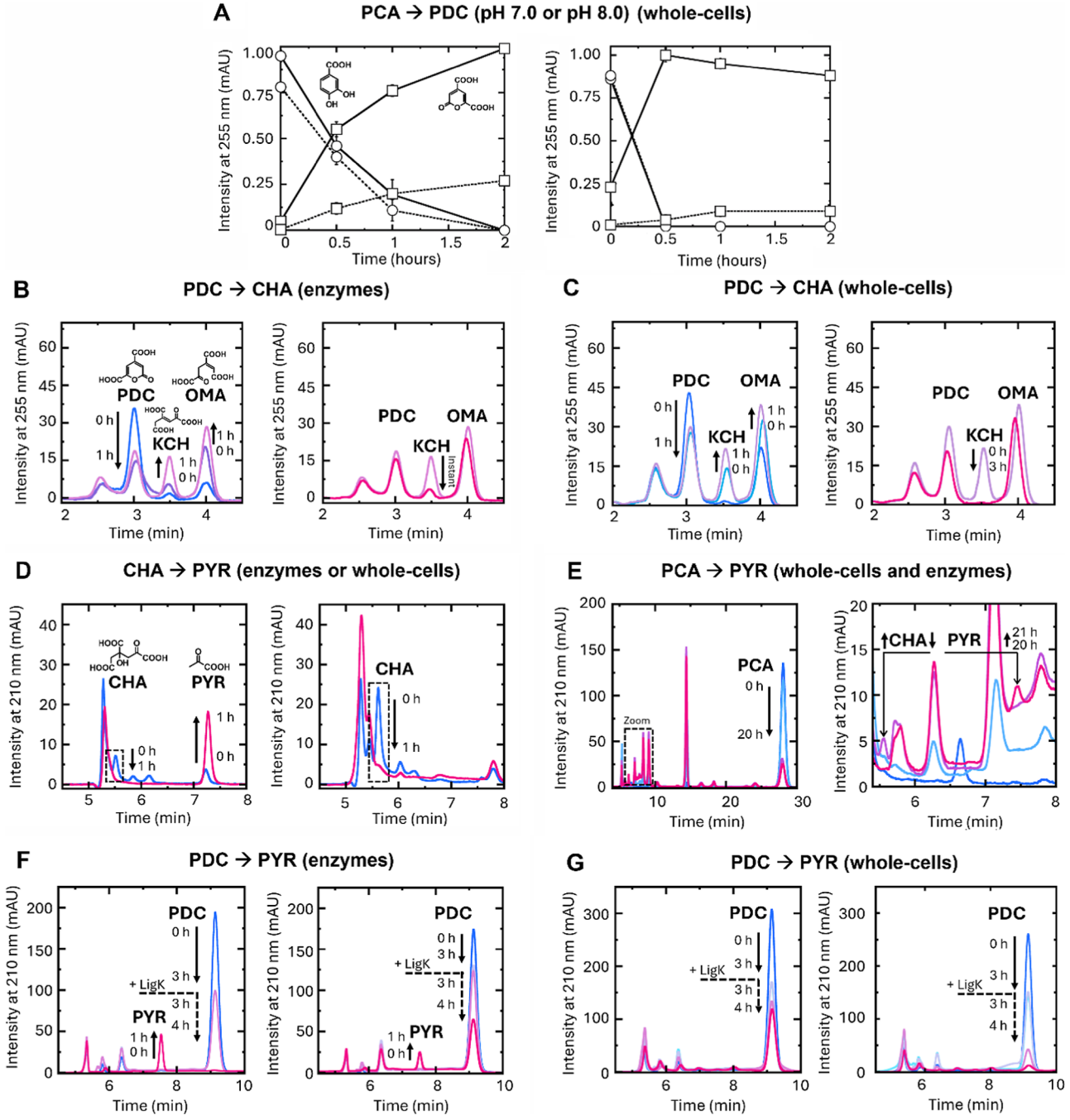

Figure 3. Setup of the bioconversion of PCA into pyruvate, at 30 °C. (A) Bioconversion of 1 mM PCA (circle) into PDC (square) using recombinant *E. coli* RARE ABC cells expressing LigAB and LigC evaluated by HPLC analysis. The left panel shows the bioconversions performed in 100 mM Tris−HCl, pH 7.0, 10% w/v glycerol with (continuous line) or without (dotted line) 1 mM $NADP^+$; the right panel shows the bioconversions performed in 100 mM Tris−HCl, pH 8.0 with (continuous line) or without (dotted lines) 1 mM $NADP^+$ (n = 3). (B) Fast protein liquid chromatography analysis of 1 mM PDC bioconversion by LigI and LigJ enzymes. The chromatograms of recombinant LigI bioconversion are reported in the left panel, while the chromatograms of the reaction mixture following the addition of LigJ are reported in the right panel. (C) Fast protein liquid chromatography analysis of the bioconversion of 1 mM PDC performed by recombinant *E. coli* cells expressing LigI and LigJ separately. The chromatograms of the bioconversion mixture using recombinant *E. coli* expressing LigI are reported in the left panel, while the ones obtained following the addition of cells expressing LigJ are reported in the right panel. (D) HPLC analysis of the bioconversion of 0.7 mM CHA. Chromatograms referring to the bioconversion performed by LigK are displayed in the left panel, while the chromatograms referring to the reaction performed by *E. coli* cells expressing LigK are reported in the right panel. (E) HPLC analysis of 1 mM PCA bioconversion by recombinant *E. coli* cells expressing LigAB, LigC, LigI, and LigJ (left panel) in which the consumption of PCA is observed in 20 h. The right panel reports a zoom-in of the bioconversion chromatogram allowing to appreciate the formation of the pyruvate peak 1 h following the addition of recombinant LigK. (F,G) Effect of LigU on the PDC bioconversion. Panel F: HPLC analysis of 1 mM PDC bioconversion into pyruvate by recombinant LigI, LigJ, and LigK enzymes (left panel), and by LigI, LigJ, LigU, and LigK (right panel): in both cases, LigK was added after 3 h. Panel G: HPLC analysis of 1 mM PDC bioconversion into pyruvate by*E. coli* RARE IJ (left panel) or RARE IUJ (right panel) strains. In both cases, the RARE K cells were added after 3 h: no signal attributable to pyruvate was detected.

https://doi.org/10.1021/acscatal.5c06530
ACS Catal. 2025, 15, 17829−17843

overexpressing the tpaK transporter (see Supporting Information and Figure S5).

Bioconversion of PCA into Pyruvate. The bioconversion of PCA into pyruvic acid (Step 3) was studied by dividing the entire six-step pathway from *Sphingobium* sp. SYK-6 into three different sections, each evaluated using a combination of different approaches.

Bioconversion of PCA into PDC. PCA is converted into PDC via two-steps (Step 3, Scheme 1): at first, 4-carboxy-2-hydroxymuconate-6-semialdehyde (CHMS) is synthesized by the protocatechuate 4,5-dioxygenase, LigAB. This intermediate is involved in an equilibrium with its hemiacetal form, which is the substrate for the subsequent oxidation mediated by the LigC enzyme, a CHMS dehydrogenase: the resulting lactonic product is PDC. The *LigAB* and *LigC* encoding genes were cloned in the high copy number pRSFDuet-1 plasmid and used to transform the *E. coli* K-12 MG1655 RARE, obtaining the *E. coli* K-12 MG1655 RARE pRSF-Duet1:LigAB_LigC (RARE ABC) strain; see Supporting Information for details on protein expression. The strategy based on whole-cells is known to better compare to the use of the recombinant enzymes due to the reported rapid inactivation of the purified LigAB by molecular oxygen.[31] One mM PCA was completely consumed within 2 h by cells at a concentration of 50 mg cww·mL^{-1}, both in 100 mM Tris−HCl buffer at pH 8.0 and at pH 7.0 supplemented with 10% (w/v) glycerol. The reaction proceeded more rapidly at pH 8.0 (Figure 3A). However, quantitative production of PDC—monitored by its characteristic absorbance at 312 nm—was achieved only when an equimolar concentration of $NADP^+$ (1 mM) was used. In contrast, using 0.1 mM $NADP^+$ or increasing the cell concentration to 100 or 200 mg cww·mL^{-1} led to the formation of only ∼0.3 and ∼0.2 mM PDC, respectively (data not shown). These findings indicate that the RARE ABC strain exhibits a limited capacity for $NADP^+$ regeneration. The PDC yield obtained with 1 mM $NADP^+$ is consistent with previous reports, such as a 95% conversion of PCA to PDC after 7 h,[29] or a molar yield of 81%.[32]

Bioconversion of PDC into CHA. The bioconversion of PDC into 4-carboxy-4-hydroxy-2-oxoadipate (CHA) proceeds through an extensive system of pH-driven equilibrium (Scheme 1). Specifically, PDC is hydrolyzed by LigI into a mixture of CHM and OMA. CHM and (4*E*)-oxalmesaconate ((4*E*)-OMA) undergo keto−enol tautomerization, along with a structural isomerization involving the C5/C4 double bond of OMA, leading to the spontaneous formation of (3*Z*)-2-keto-4-carboxy-3-hexenedioate (KCH). The final step, mediated by LigJ, involves the hydration of the double bond of KCH into CHA. These equilibria were monitored using an anion exchange chromatography method based on a fast protein liquid chromatography apparatus,[33] chosen to maintain the samples under operational conditions resembling the reaction environment, thereby preventing any equilibrium shift not attributable to the ongoing enzymatic reactions.

Regarding the bioconversion with recombinant enzymes, a sequential approach was employed. Initially, 1 mM PDC was hydrolyzed using 100 nM purified LigI under standard conditions: the reaction reached a steady ratio between the concentrations of OMA, CHM, and KCH within 1 h, with an apparent 53% PDC consumption. The resulting mixture was then processed further by adding 100 nM LigJ, which led to the immediate disappearance of the putative KCH peak (Figure 3B); the formation of CHA, as absorbance signal at 210 nm, was undetectable.

The same reaction was evaluated using different combinations of whole-cell biocatalysts. Bioconversions were carried out with *E. coli* K-12 MG1655 RARE cells, either individually or coexpressing LigI and LigJ from the medium copy plasmid pET-Duet1. The resulting biocatalysts were designed as *E. coli* K-12 MG1655 RARE:LigI (RARE I), *E. coli* K-12 MG1655 RARE pET-Duet1:LigJ (RARE J), and *E. coli* K-12 MG1655 RARE pET-Duet1:LigI_LigJ (RARE IJ). Addition of 50 mg_{cww}·mL^{-1} RARE I cells to 1 mM PDC led to the appearance of the putative peak corresponding to KCH in 1 h, which consumption was apparent 2 h after adding the RARE J cells (Figure 3C). A similar result was observed using the RARE IJ strain (not shown).

Bioconversion of CHA into Pyruvate. The bioconversion of CHA into pyruvate is a two-step decarboxylation process mediated by a single enzyme, LigK (Scheme 1). The substrate was synthesized starting from oxaloacetate (OA) using the technique reported by Wiley and Kim, 1973:[34] the resulting product, a mixture of different carboxylic acids, was reacted using both the recombinant enzyme and the whole-cell approach. In detail, a solution containing approximately 0.7 mM CHA and 0.2 mM OA was incubated with 200 nM LigK and 1 mM $MgCl_2$. Complete consumption of CHA and the formation of approximately 1.6 mM of pyruvate were observed within 1 h (Figure 3D, left), indicating full conversion of both CHA and OA. In contrast, using *E. coli* K-12 MG1655 RARE cells harboring the *ligK* gene into the low-copy number plasmid pCDF-Duet1, i.e., using the *E. coli* K-12 pCDF-Duet1:LigK (RARE K) strain (at a final concentration of 50 mg_{cww}·mL^{-1} with 1 mM $MgCl_2$), the CHA peak was cleared in 1 h, while the peak corresponding to pyruvate was not produced (Figure 3D, right). This suggests that generated pyruvate is likely consumed by cell metabolism.

Bioconversion of PCA into Pyruvate. The previously described steps were then integrated to establish a two-step bioconversion process. Initially, a whole-cell biocatalyst harboring four out of the five previously described genes was used: *E. coli* K-12 MG1655 RARE pRSF-Duet1:LigAB_LigC, pET-Duet1:LigI_LigJ (RARE ABCIJ). The complete consumption of 1 mM PCA and the formation of PDC and CHA peaks were observed within 24 h (Figure 3E, left). The addition of 200 nM LigK resulted in the complete consumption of CHA within 1 h, accompanied by the formation of a small amount of pyruvate (≈70 μM), along with residual PDC and accumulation of additional CHM intermediates (Figure 3E, right).

The conversion of CHM into KCH occurs spontaneously ($t_{1/2}$ of 59 min), but this isomerization step could become rate-limiting in the overall bioconversion process. LigU catalyzes the isomerization of OMA to the *Z* isomer of KCH (the actual substrate of LigJ, rather than OMA or its enol tautomer),[33] with a reported k_{cat} of 1300 s^{-1} and K_m of 0.17 mM at pH 8.0. When the isomerase LigU was added to the bioconversion mixture of 1 mM PDC catalyzed by 100 nM recombinant LigI and LigJ (in the presence of 1 mM $MgCl_2$), a lower residual concentration of PDC was detected within 1 h (Figure 3F, left). Notably, the subsequent addition of 100 nM LigK led to the complete PDC consumption and the formation of 2 mM pyruvate, indicating full conversion (2 molecules of pyruvate are generated from 1 molecule of CHA). In contrast, the

https://doi.org/10.1021/acscatal.5c06530
ACS Catal. 2025, 15, 17829−17843

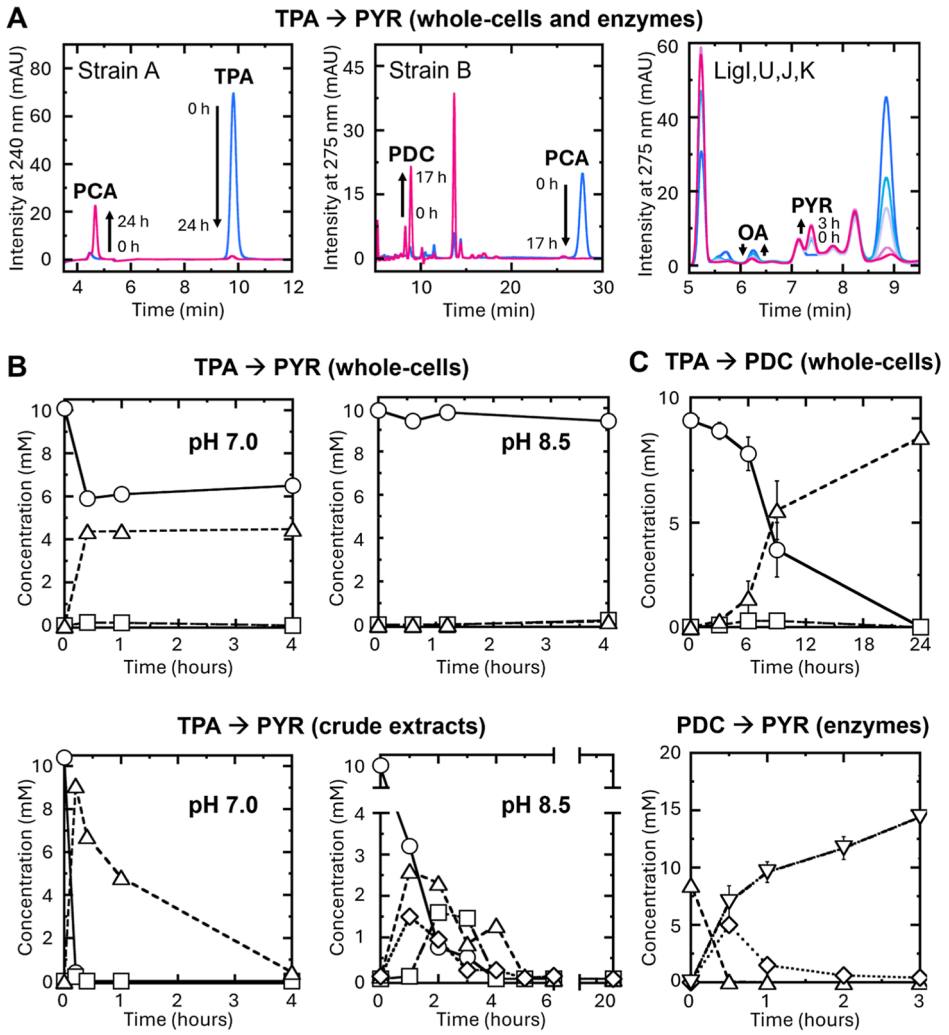

Figure 4. Optimization of the conversion of TPA into pyruvate. (A) Tandem bioconversion process at 30 °C under agitation. One mM TPA in 1 mL (left; 0 h in blue and 24 h in fuchsia), followed by bioconversion of 0.5 mM PCA in 1 mL by strain B (middle; 0 h in blue and 17 h in fuchsia), and then of the produced PDC by recombinant enzymes (right; 0 h in blue, 0.5 h in light blue, 1 h in lilac, 2 h in purple, and 3 h in fuchsia). (B) Top: Single-step bioconversion of 10 mM TPA (at 30 °C under agitation) by combined whole-cells of strain C and strain RARE K in 100 mM Tris−HCl, pH 7.0, 10% w/v glycerol (left) or 100 mM Tris−HCl, pH 8.5, 10% w/v glycerol (right). Bottom: single-step bioconversion of 10 mM TPA at 30 °C under agitation by the crude extracts of strain C and strain RARE K in 100 mM Tris−HCl, pH 7.0, 10% w/v glycerol (left) or in 100 mM Tris−HCl, pH 8.5, 10% w/v glycerol. (C) 50 mL scale-up of pyruvate production from 10 mM TPA by the two-step process employing at first the whole-cells of strain D (top) followed by recombinant LigI, LigJ, LigU, and LigK enzymes (bottom). O, TPA; □, PCA; △, PDC; ◇, OA; ▽, PYR. Error bars report the standard deviation (n = 3).

reaction mixture without LigU still retained a significant amount of unconverted PDC (Figure 3F, right).

The same bioconversions were also carried out using the whole-cell biocatalysts, namely, the RARE IJ strain or the *E. coli* K-12 MG1655 RARE pET-Duet1:LigI_LigJ, pCDF-Duet1:LigU (RARE IUJ) strains. As observed above, bioconversion using RARE IJU cells resulted in a faster PDC consumption compared with RARE IJ cells (Figure 3G, left). Furthermore, the subsequent addition of the RARE K biocatalyst (50 mg_{cww}·mL^{-1}) led to a more fast and extensive consumption of PDC compared to the bioconversion with RARE IJ alone (Figure 3G, right). As before, no detectable pyruvate signal was observed in the presence of the whole-cell biocatalysts, likely due to its use in cellular metabolism.

Bioconversion of TPA into Pyruvate. Tandem Approach Based on Whole-Cells (Strains A and B) and Recombinant LigI, J, U, K Enzymes. The conversion of TPA into pyruvate (see Steps 2 and 3, Scheme 1) was evaluated through a series of progressively optimized whole-cell reactions. First, strain A and *E. coli* K-12 MG1655 RARE pRSF-Duet1:LigAB_LigC, pET-Duet1:LigI_LigJ, and pCDF-Duet1:LigU (strain B) were evaluated to identify common bioconversion conditions. The optimal growth and induction conditions for the simultaneous production of both strains are reported in Table S4. Bioconversions were carried out individually using the two engineered strains under optimized conditions suitable for both (i.e., 50 mg_{cww}·mL^{-1} in 100 mM Tris−HCl, pH 7.0, 10% w/v glycerol, at 30 °C with agitation, see Figure S6), starting from 1 mM TPA for strain A and 1 mM PCA for strain B. The sequential "tandem" process resulted in complete transformation of 1 mM TPA into PCA by strain A within 24 h (Figure 4A, left). After cell removal by centrifugation, PCA was fully consumed by strain B in the following 24 h, resulting in a mixture of PDC, CHA, and related nondetectable intermediates (Figure 4A, middle). The final bioconversion to pyruvate was achieved by removing the cells and adding the

https://doi.org/10.1021/acscatal.5c06530
ACS Catal. 2025, 15, 17829−17843

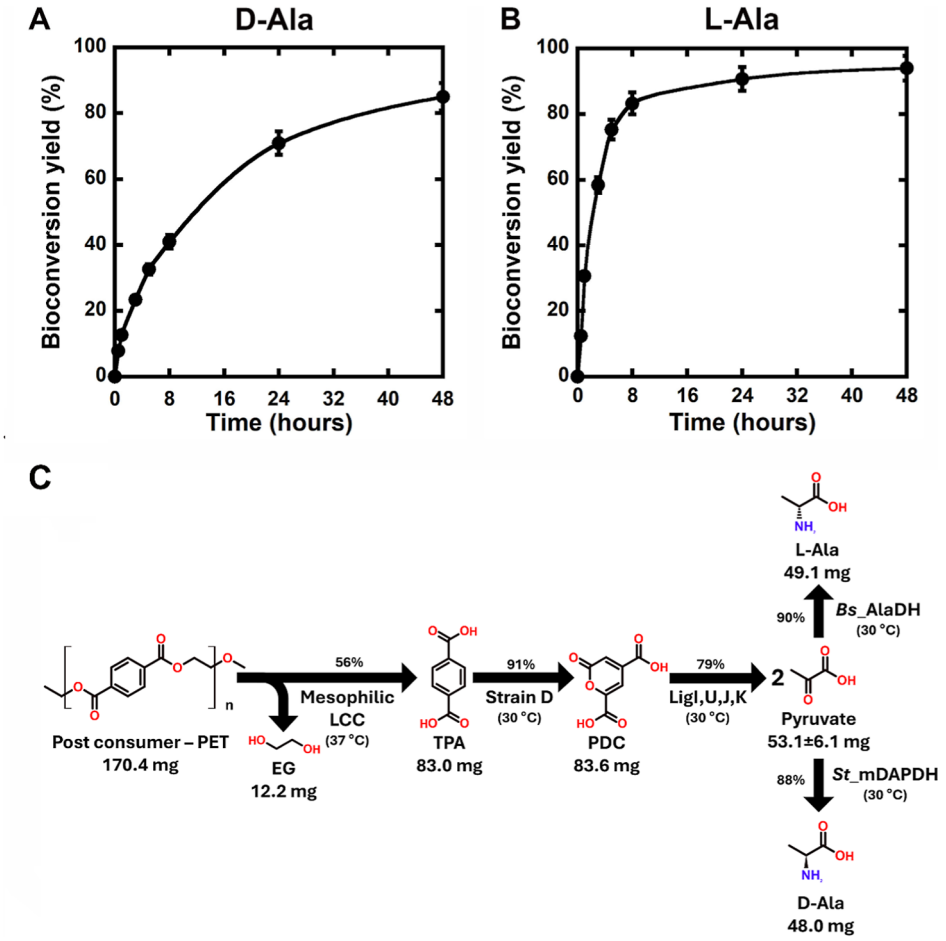

Figure 5. Production of D- and L-Ala from pyruvate. Time course of alanine production in the enzymatic conversions catalyzed by 0.1 U of (A) *St*_mDAPDH or (B) D196A/L197R_*Bs*AlaDH, in 100 mM Tris−HCl, pH 8.5, 400 mM NH_4Cl, 0.25 mM NADPH, 1 mM $MgCl_2$, 10% w/v glycerol, 100 mM glucose-6-phosphate, and 1 U glucose-6-phosphate dehydrogenase, at 30 °C (1 mL final reaction volume). The reaction mixture contained 1 mM $MgCl_2$ and 10% w/v glycerol originating from the previous reaction mixture. (C) A scheme illustrating the main steps involved in the overall conversion of postconsumer PET into D-Ala or L-Ala, along with the corresponding amounts and conversion molar yields.

recombinant enzymes (100 nM LigI, 100 nM LigJ, 100 nM LigU, 200 nM LigK, and 1 mM $MgCl_2$), resulting in a total TPA to pyruvate yield of 54.4% yield within 3 h (considering that 2 mol of pyruvate is generated from 1 mol of TPA, Figure 4A, right). Although LigI, LigU, and LigJ are already expressed in strain B, they were readded to the reaction to facilitate the equilibrium conversion between PDC, CHM, and KCH. The incomplete pyruvate production may be attributed to the high accumulation of CHMS by strain B, possibly due to a low intracellular $NADP^+$ level.

In contrast to the tandem sequential bioconversion, no TPA consumption was observed when strains A and B were used in a single-pot reaction (at either 50 or 25 $mg_{cww}{\cdot}mL^{-1}$ each), nor when strain A was combined with untransfected *E. coli* RARE cells (data not shown). No inhibition of 1 mM TPA conversion by strain A was observed in the presence of 1 mM PCA, and similarly, the conversion of 1 mM PCA by strain B was unaffected by the presence of 1 mM TPA. However, TPA consumption became evident at a higher substrate concentration: in the single-pot system with 2 mM TPA, substantial conversion occurred within 20 h. This result suggests that the presence of a second *E. coli* strain interferes with the uptake or processing of 1 mM TPA by strain A. The underlying cause of this effect warrants further investigation, as both TPA internalization and adsorption could potentially explain the observed behavior.

Strain C: Comparison between Crude Extracts and Whole-Cells. To overcome the limitations associated with the simultaneous use of strains A and B and to funnel the produced CHA into pyruvate, the feasibility of using a single biocatalyst harboring all the enzymes required for the conversion of TPA into CHA was evaluated. This was done using strain C, *E. coli* K-12 MG1655 RARE which harbored four plasmids: pET-Duet:TPADO α/β-TPADO RED, pRSF-Duet1:DCDDH_LigU, pRSF-Duet1:LigAB_LigC, and pACYC-Duet1:LigI_LigJ. These enzymes catalyze Steps 2 and 3 in Scheme 1.

For whole-cell bioconversion by strain C, the effect of TPA concentration was evaluated in the range 1−10 mM (in 100 mM Tris−HCl, pH 7.0, 1 mM $MgCl_2$, and 10% w/v glycerol). Complete TPA consumption was achieved within 24 h for concentrations up to 5 mM, whereas at 10 mM, only approximately 60% of the substrate was converted (Figure S7). A similar trend was observed when strain C and RARE K cells were used in combination. Notably, no TPA bioconversion occurred at pH 8.5 in the whole-cell system (Figure 4B, right). Interestingly, supplementation with 2 mM exogenous $NADP^+$ had no effect on TPA bioconversion by strain C, in contrast to the enhancement observed with RARE

https://doi.org/10.1021/acscatal.5c06530
ACS Catal. 2025, 15, 17829−17843

ABC cells (Figure 3A), suggesting that strain C is capable of sustaining adequate endogenous levels of the oxidized cofactor. In contrast, complete conversion of 10 mM TPA was achieved using crude extracts from strains C and RARE K at both pH 7.0 and 8.5, with a faster reaction rate observed at pH 7.0 (Figure 4B, bottom). In all cases, no pyruvate accumulation was detected, indicating that both whole-cell- and lysate-based systems efficiently metabolize oxaloacetate and/or pyruvate.

Tandem Approach Based on Whole-Cells (Strain D) and Recombinant LigI, J, U, K Enzymes. To prevent cellular metabolism from utilizing pyruvate, the overall conversion of TPA was carried out in two sequential steps. First, strain D, engineered to express TPADO α/β, TPADO RED, DCDDH, LigAB, and LigC, was used to convert TPA into PDC. Next, PDC was further converted into pyruvate using recombinant LigI, LigJ, LigU, and LigK enzymes. In the first step, 10 mM (10 μmol) of TPA generated from postconsumer PET samples (see above) was converted into 10.0 ± 0.5 mM PDC in 22 h using 50 $mg_{cww}{\cdot}mL^{-1}$ of strain D (at 30 °C, in 100 mM Tris-HCl, pH 7.0, 10% w/v glycerol). After removal of the biocatalyst and acidification to pH 2.0, PDC was isolated with a 94.7 ± 3.7% yield. PDC was then combined with 600 nM LigI, 530 nM LigJ, 550 nM LigU, 1.6 μM LigK, and 1 mM $MgCl_2$: after 3 h, a total of 13.3 mM pyruvate was produced, corresponding to an 82% TPA conversion.

A volumetric scale-up to 50 mL was carried out using 10.0 mM (83.0 mg) of TPA enzymatically derived from PET: after 24 h of incubation, the reaction mixture contained 9.1 ± 0.2 mM (83.6 mg) of PDC, corresponding to 91 ± 2% conversion yield (Figure 4C, top). The subsequent enzymatic step generated 53.1 ± 6.1 mg of pyruvate within 3 h, corresponding to 14.2 ± 1.4 mM and an overall 72 ± 7% conversion yield from TPA (Figure 4C, bottom).

Notably, the extracellular concentration of EG remained constant throughout the 24 h whole-cell bioconversion catalyzed by strain D (50 $mg_{cww}{\cdot}mL^{-1}$, at 30 °C). This suggests the potential for the valorization of EG, a coproduct of PET depolymerization product as well.

Enzymatic Conversion of Pyruvate into D-Ala and L-Ala. The last step of the bioconversion cascade involves the enzyme-mediated reductive amination of pyruvate into D-Ala or L-Ala, catalyzed by the recombinant enzymes *St*_mDAPDH and D196A/L197R_*Bs*AlaDH, respectively (Step 4, Scheme 1). In the perspective of establishing a process able to produce L-Ala, an engineered L-alanine dehydrogenase (D196A/L197R_*Bs*AlaDH) was selected in order to partially balance the cofactor consumption caused by LigC activity.[35] The switched cofactor affinity of the D196A/L197R_*Bs*AlaDH variant was successfully assessed: in comparison to the wild-type enzyme, the affinity value of the double variant on NADPH was 13-fold improved, and the one for the native cofactor NADH was decreased. The main properties of these two enzymes are reported in Tables S5 and S6 and Figure S8. Several bioconversion reactions were evaluated (see Table S7) both using commercial pyruvate and the one generated from PET. Under optimized conditions, 50 and 80 mM pyruvate were converted into D- and L-Ala in 48 h, with ≈85 and >95% yields, respectively (Figure 5A and 5B).

The bioconversion scale-up was carried out using 10 mM commercial pyruvate in a final reaction volume of 25 mL: the substrate was converted into D-Ala or L-Ala with yields of 95.3 ± 2.1% and 98 ± 1.4%, respectively, after 24 and 8 h of incubation. Both D-Ala and L-Ala were recovered from the reaction mixture by ion exchange chromatography with final yields of 88% and 90%, respectively. Specifically, 19.6 mg of D-Ala and 20.0 mg of L-Ala were recovered starting from 22 mg of pyruvate. Notably, when pyruvate generated directly from the PET degradation reaction mixture—i.e., without any intermediate purification—was used under the same conditions, the bioconversions yielded comparable results: 20.1 mg of D-Ala or 19.8 mg of L-Ala were recovered from the reaction mixture. The quantities of L-Ala and D-Ala obtained starting from 170 mg of postconsumer PET (see above) are reported in Figure 5C.

CONCLUSIONS

Unsustainable use and disposal of plastics have led to persistent and widespread environmental contamination. Within the context of a circular economy for plastics, the conversion of waste-derived PET to valuable compounds is of great interest. A plethora of compounds can be generated from the PET degradation. In this study, we focus on a novel pathway that converts TPA generated from PET enzymatic degradation into PCA and then into PDC, which undergoes ring cleavage to ultimately transform into pyruvate, thus producing D-Ala or L-Ala (Scheme 1). Consequently, the biotechnological process utilizing these microorganisms and enzymes enables both PET depolymerization and upcycling simultaneously.

The use of the microorganisms known to hydrolyze PET is not feasible due to their difficulty in cultivation or lack of proper classification. Furthermore, the biological oxidation of PET monomers to CO_2 prevents their upcycling to high-added value chemicals. To address this challenge, we engineered LCC for the enzymatic biodegradation of PET at lower temperatures compared to those normally used (close to the glass transition temperature of PET, i.e., 72 °C, and no lower than 50−55 °C).[10,36] Up to now, the LCC^{ICCG} variant is the most promising enzyme for industrial-scale PET recycling, achieving 98% PET conversion within 24 h at 68 °C, with an average productivity of 5.8 g TPA/L/h and a maximum of 28.6 g TPA/L/h.[24] Our approach was designed to be compatible with subsequent bioconversion steps and to produce a less energy-intensive process. In this study, we identified the mesophilic S101N/F243T-ΔLCC variant, which demonstrated reasonable depolymerization activity on a PET film at 37 °C (Figure 1): after 21 days of incubation, 85% of the polymer was converted into TPA with no loss of enzymatic activity (Figure 1F). TPA was also produced from postconsumer PET waste samples, with depolymerization yield >50%.

The conversion of TPA into pyruvate was optimized using whole-cells and recombinant enzymes in a tandem system approach (Steps 2 and 3 in Scheme 1). In particular, the low yield due to the equilibrium between PDC products was resolved by adding LigU isomerase. These studies revealed that pyruvate cannot be accumulated into *E. coli* cells due to its immediate use: consequently, strain D (encoding TPADO α/β, TPADO RED, DCDDH, LigAB, and LigC) was used to convert TPA into PDC—overcoming the inherent stability limitations of certain purified enzymes—and the subsequent steps were carried out using recombinant LigI, LigJ, LigU, and LigK enzymes. The conversion of 10 mM TPA derived from postconsumer PET was scaled up to a 50 mL volume, generating 51 mg of pyruvate from 66 mg of TPA. Finally, the conversion into the targeted value-added products, L-Ala or D-Ala, was carried out using a variant of *Bs*AlaDH and

https://doi.org/10.1021/acscatal.5c06530
ACS Catal. 2025, 15, 17829−17843

*St*_mDAPDH, respectively (Step 4 in Scheme 1): specifically, 50 mM pyruvate was converted into D-Ala in 48 h with an ≈85% yield, and 80 mM pyruvate was converted into L-Ala in 24 h with a >95% yield (Figure 5A,B). Overall, under optimal conditions, 48−49 mg of L-Ala or D-Ala were generated from 170 mg of untreated postconsumer PET (Figure 5C).

Metabolic engineering studies have demonstrated that microorganisms such as *P. putida* and *C. glutamicum* can be tailored to efficiently utilize aromatic substrates and TPA derived from PET for the biosynthesis of value-added compounds.[37−39] Notably, *Pseudomonas* strains are renowned for their robust β-ketoadipate pathway, which enables the assimilation of lignin-derived aromatic monomers such as catechol and PCA into central carbon metabolism, yielding key intermediates such as pyruvate: the replacement of the native ortho-cleavage pathway in *P. putida* KT2440 with a meta-cleavage route led to a 31% (w/w) and 59% (w/w) pyruvate yield, using catechol and PCA as substrates, respectively.[37] However, to date, no study has reported the direct production of D- or L-Ala from aromatic compounds using metabolically engineered microorganisms, including *Pseudomonas* species. Current alanine-producing platforms remain largely fermentative and glucose-based, achieving high titers and yields. Engineered *E. coli* strains have reached 114 g L^{-1} L-Ala with a yield of 0.95 g g^{-1} glucose, while *C. glutamicum* strains engineered for L-Ala production achieved 98 g L^{-1} with 0.83 g g^{-1} glucose.[19] More recently, *C. glutamicum* has been metabolically engineered for D-Ala biosynthesis, reaching 85 g L^{-1} with a yield of 0.30 g g^{-1} glucose.[20] These systems clearly demonstrate the potential for high-efficiency alanine fermentation but depend on high sugar concentrations and extensive genetic and metabolic rewiring to redirect carbon flux and minimize byproduct formation.[19,20] In this context, the hybrid enzymatic and whole-cell system developed in this study represents, to the best of our knowledge, the first platform enabling the selective synthesis of enantiopure D- and L-Ala from PET-derived aromatics.

The primary limitation of the proposed process is the requirement to employ both cellular and enzymatic systems, which adds to the complexity of a potential preparative system. At the same time, the system is modularly structured, thus offering fine control over reaction conditions and enantiomeric selectivity while also enabling the application of individual components to different processes in line with a modular design approach to biocatalytic systems.

TPA derived from PET degradation is a high-value product, with an annual global production of 40 million metric tons and a market value of $46 billion as of 2023, along with a projected CAGR of 5.03% from 2024 to 2034.[40] Furthermore, future efforts should focus on identifying and harnessing alternative protein sources to meet rising global food demand while reducing the environmental footprint of conventional agriculture. This bioconversion pathway offers a sustainable and efficient solution to the amino acid supply. Given the commercial cost of PET at approximately $1.2/kg and the current market prices for amino acids—ranging from $3 to 15/kg for bulk L-Ala, $30 to 40/kg for food-grade L-Ala, and $450 to 900/kg for pharmaceutical-grade L-Ala, or $10 to 30/kg for bulk D-Ala and up to $800−1200/kg for pharmaceutical-grade D-Ala[41,42]—this process represents a substantial value upgrade for PET.

An additional value is evident with the environmental benefits of eliminating a hazardous compound. PET, and especially PET microplastics (widely present in wastewater and causing adverse effects in ecosystems, aquatic life, and ultimately, humans), can be converted into useful compounds through a sustainable approach, addressing the challenges posed by plastics throughout their entire life cycle. This process aligns with many of the United Nations' "Sustainable Development Goals" for 2030. In conclusion, optimizing production levels and expanding the range of products generated from PET depolymerization through biological upcycling are highly desirable goals and targets for future studies. Furthermore, the underlying concepts and strategies employed in this work are potentially applicable to the treatment of other plastics and feedstocks, providing valuable insights into the development of a sustainable bioeconomy.

METHODS

Strains, Plasmids, and Reagents. All of the strains used in this work are listed in Table S2. Competent NEB 10-beta (BioLabs Inc.) and JM109 *E. coli* strains were employed for gene cloning and plasmid propagation, *E. coli* BL21(DE3) cells were used for recombinant protein expression, and *E. coli* K-12 MG1655 RARE (reduced aromatic aldehyde reduction, bacterial strain #61440, Addgene, Watertown, USA) cells were used for whole-cell bioconversions. All the plasmids used in this work are listed in Table S3. The sequences of all constructed plasmids were verified using DNA sequencing (Eurofins genomics).

Methanol (ACS grade, ≥99%), formic acid (ACS grade, ≥98%), acetonitrile (ACS grade), *p*-nitrophenyl acetate (*p*-NPA), nicotinamide adenine dinucleotide phosphate tetrasodium salt reduced form (NADPH, ≥98%), and nicotinamide adenine dinucleotide (NAD^+, ≥98%) were purchased from Merck/Carlo Erba (Merck KGaA, Darmstadt, Germany); nicotinamide adenine dinucleotide phosphate disodium salt oxidized form ($NADP^+$, 98%) was purchased from Boehringer GmbH (Mannheim, Germany). Analytical-grade standard of disodium terephthalate salt (≥99%, 1,4-benzenedicarboxylic acid, TPA) was purchased from TCI (Tokyo Chemical Industry Co.), analytical-grade standard of protocatechuic acid (3,4-dihydroxybenzoic acid, PCA) was purchased from Thermo Scientific Chemicals.

PET nanoparticles were prepared from PET microplastic (diameter 300 μm; Goodfellow GmbH, Bad Nauheim, Germany) using a precipitation and solvent evaporation technique.[10] PET nanoparticles showed a mean diameter of 80 nm (as determined by dynamic light scattering) and a concentration of 630 ± 80 μg mL^{-1}. Amorphous PET film was purchased from Goodfellow Cambridge Ltd. (Huntingdon, UK, 250 μm thick, product number ES301445).

Evolution of a Mesophilic LCC Variant. For this work, the libraries of ΔLCC (a deleted form of LCC lacking the 34 residue-long N-terminal secretion signal) generated by Pirillo et al., 2023,[10] were used. In detail, SSM was carried out at positions 95, 96, 127, 212, and 243 using the QuickChange II XL Site-directed mutagenesis kit (Agilent Technologies, Santa Clara, CA, USA), the gene-encoding ΔLCC as a template, and the primers carrying NNK-degenerate codons at the desired positions (i.e., degenerated primers with N = A, C, G, or T and K = G or T, see Table S8). The amplification mixture was used to transform *E. coli* NEB 10-β cells, obtaining libraries of approximately 3000 clones each. SSM was also carried out at positions 97 and 101 using the gene-encoding F243T-ΔLCC as a template.

https://doi.org/10.1021/acscatal.5c06530
ACS Catal. 2025, 15, 17829−17843

The plasmid DNA pools containing the whole genetic variability generated by SSM were transferred to the BL21(DE3) *E. coli* expression strain to screen the enzymatic activity under both mesophilic and thermophilic conditions. This innovative screening is based on an activity assay carried out at 37 °C to identify mesophilic enzyme variants, also performed following 1 h of incubation at a high temperature (80 °C) to isolate those variants retaining thermophilic stability. The screening was conducted using a colorimetric assay employing the PSP dye and using the OT-2 automated liquid-handling system (Opentrons Labworks, Inc., New York, USA).[43] This assay allows measurement of the pH change associated with the TPA production from PET depolymerization. A 0.1 mM final concentration of isopropyl β-D-1-thiogalactopyranoside (IPTG) was added to 1 mL of *E. coli* cultures grown at saturation in deep-well plates at 37 °C and the cells were incubated at 17 °C for 18 h. One mL of each culture was centrifuged, the pellet was resuspended with 0.3 mL of lysis solution (1 mM Na_2HPO_4, pH 8.1, 100 mM NaCl, 40 $\mu g \cdot mL^{-1}$ lysozyme) and incubated for 30 min at 37 °C. To identify the mesophilic variants, crude extracts (50 μL) were transferred into a 96-well plate. The hydrolytic activity was assayed by adding 0.1 mg of PET nanoparticles and 0.2 mM PSP. After incubation at 37 °C for 3 h, the absorbance at 540 nm was recorded by a microtiter plate reader (Infinite 200, Tecan) and compared with the figure for cells expressing the ΔLCC (positive control) and cells transformed with the pET24b(+) empty vector (negative control). On the other hand, the identification of thermostable variants also active at 37 °C was conducted by incubating crude extracts transferred into a 96-well plate (50 μL) at 80 °C for 1 h. After cooling down at room temperature for 15 min, the hydrolytic activity was assayed as stated above. Clones showing a significant activity at 37 °C were confirmed by a second screening, and the ΔLCC genes coding for the most interesting variants were sequenced (Eurofins Genomics).

Production of LCC Variants. The synthetic gene-encoding S101N/F243T-ΔLCC variant was produced by Pirillo et al., 2023.[10] For protein production, the gene was subcloned into the pET24b(+) expression vector (between *Nde*I and *Xho*I restriction sites) and expressed into the Origami2(DE3) *E. coli* strain. Briefly, 1 L of Luria−Bertani (LB) broth medium supplemented with 12.5 $\mu g \cdot mL^{-1}$ tetracycline and 30 $\mu g \cdot mL^{-1}$ kanamycin was grown at 37 °C, and 0.1 mM IPTG was added and incubated for 18 h at 17 °C. Cells were harvested by centrifugation and lysed by sonication. The crude extract was recovered by centrifugation and loaded onto a 1 mL HiTrap chelating-affinity column (Cytiva, Marlborough, MA, USA) equilibrated in binding buffer (50 mM Tris−HCl, 500 mM NaCl, 20 mM imidazole, pH 8.0) and preloaded with 100 mM $NiCl_2$. ΔLCC was eluted with 50 mM Tris−HCl, 200 mM NaCl, and 500 mM imidazole (pH 8.0) and equilibrated in 25 mM Tris−HCl, 200 mM NaCl (pH 8.0) using a PD-10 desalting column (Cytiva). ΔLCC concentration was estimated based on the theoretical extinction coefficient at 280 nm of 38453 $M^{-1} \cdot cm^{-1}$. The same protocol was used to express and purify the ΔLCC variants generated by SSM.

The reference hydrolytic enzymatic activity was measured on 1 mM *p*-NPA by a spectrophotometric assay at 30 °C in 50 mM disodium phosphate, 100 mM NaCl (pH 8.0) recording the absorbance increase at 405 nm due to the product *p*-nitrophenolate (ε_{405} = 14.4 $mM^{-1} \cdot cm^{-1}$).[44] One unit (U) of esterase activity was defined as the amount of enzyme that releases 1 μmol of *p*-nitrophenolate per minute under the assay conditions described. Activity on PET nanoparticles was measured using a turbidimetric assay. PET nanoparticles (∼94 $\mu g \cdot mL^{-1}$) were incubated in 25 mM Tris−HCl, 200 mM NaCl (pH 8.0), at 30, 37, or 50 °C with 20 $\mu g \cdot mL^{-1}$ enzyme; the reaction mixture was mixed and incubated for 10 min in a cuvette. The turbidity (OD_{600nm}) was recorded every 10 s using a Jasco V-560 spectrophotometer (Jasco Inc., Easton, MD, USA).[10]

Design and cloning of genes encoding each enzyme of the pathway, protein expression conditions, and yields are reported as Supporting Information (see Tables S9 and S10 and Figures S9−S19).

Cultivation of the Whole-Cell Biocatalysts and Crude Extract Preparation. The whole-cell biocatalysts of Steps 2 and 3 (Scheme 1), as well as the different combinations of biocatalysts (see below), were prepared by inoculating a single colony of the recombinant *E. coli* MG1655 RARE strains into 100−200 mL of LB broth medium supplemented with the appropriate antibiotic combinations (30 $\mu g \cdot mL^{-1}$ kanamycin, 100 $\mu g \cdot mL^{-1}$ ampicillin, 50 $\mu g \cdot mL^{-1}$ streptomycin, and/or 34 $\mu g \cdot mL^{-1}$ chloramphenicol) and grown at 30 °C. Once the OD_{600nm} of the cultures reached a value of approximately 0.6, 1 mM IPTG was added, and cultures were incubated for 3 h at 30 °C; cells were harvested by centrifugation (8000*g*, 4 °C, 10 min). Cell pellets were resuspended in the bioconversion buffer (100 mM Tris−HCl, pH 7.0, 10% w/v glycerol) to a final concentration of 500 $mg_{cww} \cdot mL^{-1}$ and stored at 4 °C. The same protocol, followed by the harvesting and resuspension steps, was performed for not transformed *E. coli* MG1655 RARE cells and *E. coli* MG1655 RARE transformed with empty plasmids as a control of the bioconversion reactions. The presence of one or multiple plasmids for the expression of the different enzymes affected to a minor extent the growth of the *E. coli* MG1655 RARE cells: a quite similar final OD_{600nm} figure was obtained after 3 h from IPTG addition (Figure S20).

When required, crude extracts were obtained by disrupting the resuspended cell pellets by sonication, followed by centrifugation (39,000*g* for 1 h at 4 °C) and then storing at 4 °C.

Whole-Cell Biotransformation. Different combinations of plasmids were introduced into the *E. coli* MG1655 RARE strain through chemical transformation to construct the whole-cell biocatalysts (see Table S2).

Bioconversion of the PET Film into TPA (Step 1). PET film (Goodfellow Cambridge Ltd., Huntingdon, UK, 250 μm thick, amorphous) was cut into disks of 6 mm in diameter (corresponding to ≈7 mg) and washed with 0.1% SDS, ethanol, and deionized water, followed by drying at 50 °C for 1 h. Various transparent and untreated postconsumer PET wastes (i.e., a candy tray and a cheesecake lid) were also cut into disks of 6 mm in diameter (corresponding to ≈5−8 mg, depending on the sample) and washed as above. The S101N/F243T-ΔLCC variant (40 $\mu g \cdot mL^{-1}$) was added to 1 mL of 7 mg mL^{-1} PET film in 100 mM Tris−HCl, pH 8.0 at 37 °C. An untreated and transparent postconsumer PET waste (cheesecake lid, ≈0.5 g) was washed as previously stated and added to 15 $\mu g \cdot mL^{-1}$ of the S101N/F243T-ΔLCC variant in 100 mL of 100 mM Tris−HCl, pH 8.0 at 37 °C. The generated reaction mixture was used to setup a large-scale bioconversion.

The PET depolymerization products generated by S101N/F243T-ΔLCC (i.e., TPA and MHET) were recorded by

https://doi.org/10.1021/acscatal.5c06530
ACS Catal. 2025, 15, 17829−17843

spectrophotometric analysis. The concentration of the soluble aromatics was determined from the absorbance at 240 nm ($\varepsilon_{240\ nm}$ of 13260 $M^{-1}cm^{-1}$).[35] Reaction products were also analyzed by HPLC (see below).

Bioconversion of TPA into PCA (Step 2). To evaluate the bioconversion of TPA into PCA, a whole-cell reaction was set up using the recombinant *E. coli* MG1655 RARE cells (100 $mg_{cww}\cdot mL^{-1}$) expressing both pET-Duet:TPADO α/β-TPADO RED and pRSFDuet:DCDDH. The reaction was performed in a final volume of 500 μL, into a 50 mL tube to ensure appropriate oxygenation[12] and it was carried out in 100 mM Tris−HCl, pH 7.0, 10% w/v glycerol as the bioconversion buffer. One millimolar of analytical-grade TPA (as disodium salt) was incubated at 30 °C for up to 24 h with the whole-cell biocatalyst. One mL of the reaction mixture from Step 1 was also used as a substrate for the whole-cell reaction. 10% w/v glycerol was added prior to the addition of the biocatalyst (50 $mg_{cww}\cdot mL^{-1}$). Reaction products were analyzed by HPLC (see below).

Bioconversion of PCA into Pyruvate (Step 3). The whole-cell biotransformations were performed using analytical-grade substrates and the recombinant RARE ABCIJ *E. coli* cells (50 $mg_{cww}\cdot mL^{-1}$) or the respective crude extract, in either 100 mM Tris−HCl, pH 8.0, or 100 mM Tris−HCl, pH 7.0, 10% w/v glycerol. The reactions were carried out in 1 mL final volume, into a 50 mL Falcon tube to ensure an adequate oxygenation. All reactions were performed at 30 °C on a rotatory shaker. The processes were monitored by withdrawing at different times 10 μL of the reaction mixture, immediately diluted in 90 μL of 5 mM sulfuric acid and centrifuged for 10 min at 16,000*g*, 4 °C, to remove the cells. Twenty microliters of the supernatant were analyzed by HPLC (see below).

Bioconversion of Pyruvate into D-Ala and L-Ala and Scale-Up (Step 4). The enzymatic bioconversions were set up using 50 or 80 mM analytical-grade pyruvate and the recombinant enzymes *St*_mDAPDH (0.1 U, 0.5 mg) or D196A/L107R-*Bs*AlaDH (0.1 U, 5 μg), respectively, in 100 mM Tris−HCl, pH 8.5, 400 mM NH_4Cl, 0.25 mM NADPH, 1 mM $MgCl_2$, 10% w/v glycerol, 100 mM glucose-6-phosphate, and 1 U glucose-6-phosphate dehydrogenase (200 U/mg). The reactions were carried out in a 1 mL final volume, at 30 °C on a rotatory shaker. The reaction controls were performed in the absence of enzymes. At different times, 20 μL were withdrawn for HPLC analyses (see below). The scale-up of the bioconversion was performed under the same operational conditions using 10 mM analytical-grade pyruvate in a 25 mL reaction mixture containing *St*_mDAPDH (0.5 U, 2.5 mg) and D196A/L107R-*Bs*AlaDH (0.5 U, 25 μg), respectively.

Products' Identification. For the identification of the reaction products of Steps 1 and 2 (Scheme 1), HPLC analyses were performed on a Jasco LC-4000 system equipped with a Symmetry C18 column (4.6 mm × 250 mm, Waters) or a Bischoff PRONTOGEL H (ion-exchange column 300 mm × 8.0 mm, pore size 10 μm, Leonberg, Germany). Regarding the separative analyses performed using the Symmetry C18 column, the mobile phase was 60% v/v 0.1% formic acid in Milli-Q, 40% v/v methanol. The elution was isocratic at a flow rate of 0.8 $mL\cdot min^{-1}$ and the oven temperature was 35 °C. The compounds were detected by recording the absorbance at 240 nm. All samples were prepared by dilution with the mobile phase and centrifugation (10 min, 16,000*g*, 4 °C) to remove the biocatalyst before injection. Twenty microliters of the supernatant were analyzed. The retention times of PCA and TPA were 4.7 and 9.5 min, respectively: concentrations were evaluated by means of calibration lines (0.01−0.1 mM) prepared with TPA and PCA (Figure S21).

Regarding the analyses with the Bischoff PRONTOGEL H system, the separation was performed operating an isocratic elution in 5 mM sulfuric acid at a flow rate of 0.8 $mL\cdot min^{-1}$ and 50 °C. The detection of the EG and TPA generated from the depolymerization of amorphous PET film samples was performed with a Jasco RI-4030 refractive index detection system. The compounds' concentration was determined by means of calibration lines (0.3125−5 mM, Figure S22) generated by solubilizing analytical standards in 100 mM Tris−HCl, pH 8.0 and further diluted in 5 mM sulfuric acid. Retention times for standards of EG and TPA were 12.4 and 47.0 min, respectively. The compounds generated in Step 2 (Scheme 1) were detected recording the absorbance at two different wavelengths: 240 and 275 nm for PCA and TPA, respectively, and their concentration was evaluated by means of calibration line (0.0625−0.1 mM range)-generated solubilizing standards of each compound in 5 mM sulfuric acid (Figure S23). Retention times for PCA and TPA were 28 and 47 min, respectively.

For the identification of the reaction products of Step 3 (Scheme 1), HPLC analyses were performed on a Jasco LC-4000 system equipped with a Bischoff PRONTOGEL H column operating as detailed above. The compounds were detected recording the absorbance at three different wavelengths (210, 275, and 312 nm) for pyruvic acid, PDC, PCA, TPA, and OA, and quantified by means of calibration curves (Figure S23). Retention times for standards of pyruvic acid, PDC, PCA were 7.5, 9.5, and 28 min, respectively.

The production of D-Ala and L-Ala (Step 4, Scheme 1) was analyzed using a Jasco LC-4000 system equipped with a Chirobiotic T column (4.6 mm × 250 mm, Astec). The separation was carried out using isocratic elution in 70% (v/v) methanol in Milli-Q, at a flow rate of 0.8 $mL\cdot min^{-1}$, at 30 °C. The compounds were detected recording the absorbance intensity at 210 nm and quantified by means of calibration lines (0.085−16.67 mM) (Figure S24) prepared dissolving standards of each compound in 70% (v/v) methanol. The retention times for standards L-Ala and D-Ala were 5.5 and 7.4 min, respectively.

For D-Ala and L-Ala purification, the reaction mixtures were acidified to pH <2.0 by adding 10% (w/v) H_2SO_4 and centrifuged for 10 min at 16,000*g*, 4 °C, to remove insoluble components. The supernatant was loaded onto ion exchange chromatography (Dowex 50W) equilibrated with 10% H_2SO_4. The resin was washed repeatedly with deionized water and D-Ala or L-Ala was eluted with 10% (w/v) NH_4OH: the solvent was subsequently removed by evaporation.

Analysis of Reaction Intermediates. The progression of the reactions for synthesis of CHMS from PCA and of CHA from OA was tracked via LC−MS with a Waters 600 HPLC system, using a SynergiTM 4 μm Fusion RP 80 Å (150 × 4.6 mm) at a 1 $mL\cdot min^{-1}$ flow rate, coupled with a Waters MicroMass ZQ mass spectrometer and an ESI ion source (see Figures S25 and S27 for details). HPLC purification of PDC was performed on a SHIMADZU LC-20AP equipped with an FRC-10A fraction collector and SPD-M20A diode-array detector, using a SepaChrom Robusta 100 Å C18 5 μm (250 × 21.2 mm) with a 15 $mL\cdot min^{-1}$ flow rate. For freeze-drying, the product was dissolved in water and frozen with dry ice and then lyophilized for at least 48 h at −55 °C using the

https://doi.org/10.1021/acscatal.5c06530
ACS Catal. 2025, 15, 17829−17843

Telstar-LyoQuest instrument. High-resolution mass spectra (HRMS) of PDC was obtained using a Thermo Fisher Scientific Orbitrap Exploris 120 equipped with UHPLC and C18 column (see Figure S26B for details).

■ ASSOCIATED CONTENT

Supporting Information

The Supporting Information is available free of charge at https://pubs.acs.org/doi/10.1021/acscatal.5c06530.

Details about the screening procedure to identify evolved LCC variants; production of LCC as extracellular protein; *E. coli* strains and plasmids used in this study; expression conditions for the use of strains A and B in the bioconversion process; kinetic parameters of *Bs*AlaDH and *St*_mDAPDH on pyruvate, NADPH, and NH_4Cl and T_m values; reaction conditions for conversion of pyruvate into D- and L-Ala; design and cloning of genes encoding the enzymes of the pathway; list of primers used for SSM of ΔLCC; list of synthetic genes used in this study; levels of production of enzymes of the pathway; HPLC analyses of bioconversion of TPA into PCA by strain A and of PCA into PDC by strain B; time course of bioconversion of TPA into PDC by strain C; effect of temperature and pH on the enzymatic activity of *Bs*AlaDH and *St*_mDAPDH; SDS-PAGE analysis of recombinant purified enzymes of the pathway; growth curves for *E. coli* strain D; HPLC calibration lines; mass spectral analysis of product intermediates and CHA synthesis (PDF).

■ AUTHOR INFORMATION

Corresponding Authors

Elena Rosini − *Department of Biotechnology and Life Sciences, University of Insubria, 21100 Varese, Italy;* orcid.org/0000-0001-8384-7992; Phone: +39 0332421518; Email: elena.rosini@uninsubria.it

Loredano Pollegioni − *Department of Biotechnology and Life Sciences, University of Insubria, 21100 Varese, Italy;* orcid.org/0000-0003-1733-7243; Phone: +39 0332421506; Email: loredano.pollegioni@uninsubria.it

Authors

Caren Battaglia − *Department of Biotechnology and Life Sciences, University of Insubria, 21100 Varese, Italy*

Davide Miani − *Department of Biotechnology and Life Sciences, University of Insubria, 21100 Varese, Italy*

Filippo Molinari − *Department of Biotechnology and Life Sciences, University of Insubria, 21100 Varese, Italy*

Federico Arrigoni − *Department of Science and High Technology, University of Insubria, 22100 Como, Italy*

Umberto Piarulli − *Department of Science and High Technology, University of Insubria, 22100 Como, Italy;* orcid.org/0000-0002-6952-1811

Gianluca Molla − *Department of Biotechnology and Life Sciences, University of Insubria, 21100 Varese, Italy*

Complete contact information is available at: https://pubs.acs.org/10.1021/acscatal.5c06530

Author Contributions

§E.R., C.B., and D.M. have contributed equally. L.P.: conceptualization, methodology, validation, supervision, writing—original draft, writing—reviewing and editing, funding acquisition; C.B.: methodology, investigation, visualization, writing—original draft; D.M.: methodology, investigation, visualization, writing—original draft; F.M.: methodology, investigation; F.A.: methodology, investigation, visualization, writing—original draft; U.P.: methodology, supervision, writing—original draft; G.M.: conceptualization, methodology, supervision, writing—original draft, funding acquisition; E.R.: conceptualization, methodology, supervision, investigation, validation, writing—original draft.

Notes

The authors declare no competing financial interest.

■ ACKNOWLEDGMENTS

L.P., G.M., and E.R. thank the support of Fondazione Cariplo (Economia Circolare_2022), project ProPla: proteins from plastics, no. 2022-0631. C.B. and D.M. were students of the PhD course "Life Sciences and Biotechnology", University of Insubria. All the authors thank the support from Fondo di Ateneo per la Ricerca, University of Insubria.

■ REFERENCES

(1) Leslie, H. A.; van Velzen, M. J. M.; Brandsma, S. H.; Vethaak, A. D.; Garcia-Vallejo, J. J.; Lamoree, M. H. Discovery and quantification of plastic particle pollution in human blood. *Environ. Int.* **2022**, *163*, 107199.

(2) Cverenkárová, K.; Valachovičová, M.; Mackuľak, T.; Žemlička, L.; Bírošová, L. Microplastics in the food chain. *Life* **2021**, *11*, 1349.

(3) Sulaiman, S.; You, D. J.; Kanaya, E.; Koga, Y.; Kanaya, S. Crystal structure and thermodynamic and kinetic stability of metagenome-derived LC-cutinase. *Biochemistry* **2014**, *53*, 1858−1869.

(4) Yoshida, S.; Hiraga, K.; Takehana, T.; et al. A bacterium that degrades and assimilates poly(ethylene terephthalate). *Science* **2016**, *351*, 1196−1199.

(5) Han, X.; Liu, W.; Huang, J. W.; Ma, J.; Zheng, Y.; Ko, T. P.; Xu, L.; Cheng, Y. S.; Chen, C. C.; Guo, R. T. Structural insight into catalytic mechanism of PET hydrolase. *Nat. Commun.* **2017**, *8*, 2106.

(6) Austin, H. P.; Allen, M. D.; Donohoe, B. S.; Rorrer, N. A.; Kearns, F. L.; Silveira, R. L.; Pollard, B. C.; Dominick, G.; Duman, R.; El Omari, K.; et al. Characterization and engineering of a plastic-degrading aromatic polyesterase. *Proc. Natl. Acad. Sci. U.S.A.* **2018**, *115*, E4350−E4357.

(7) Amalia, L.; Chang, C. Y.; Wang, S. S.; Yeh, Y. C.; Tsai, S. L. Recent advances in the biological depolymerization and upcycling of polyethylene terephthalate. *Curr. Opin. Biotechnol.* **2024**, *85*, 103053.

(8) Liu, F.; Wang, T.; Yang, W.; Zhang, Y.; Gong, Y.; Fan, X.; Wang, G.; Lu, Z.; Wang, J. Current advances in the structural biology and molecular engineering of PETase. *Front. Bioeng. Biotechnol.* **2023**, *11*, 1263996.

(9) Pirillo, V.; Orlando, M.; Tessaro, D.; Pollegioni, L.; Molla, G. An efficient protein evolution workflow for the improvement of bacterial PET hydrolyzing enzymes. *Int. J. Mol. Sci.* **2022**, *23*, 264.

(10) Pirillo, V.; Orlando, M.; Battaglia, C.; Pollegioni, L.; Molla, G. Efficient polyethylene terephthalate degradation at moderate temperature: a protein engineering study of LC-cutinase highlights the key role of residue 243. *FEBS J.* **2023**, *290*, 3185−3202.

(11) Kim, H. T.; Kim, J. K.; Cha, H. G.; et al. Biological valorization of poly(ethylene terephthalate) monomers for upcycling waste PET. *ACS Sustain. Chem. Eng.* **2019**, *7*, 19396−19406.

(12) Sadler, J. C.; Wallace, S. Microbial synthesis of vanillin from waste poly(ethylene terephthalate). *Green Chem.* **2021**, *23*, 4665−4672.

(13) Molinari, F.; Pollegioni, L.; Rosini, E. Whole-cell bioconversion of renewable biomasses-related aromatics to cis,cis-muconic acid. *ACS Sustain. Chem. Eng.* **2023**, *11*, 5802.

(14) Kim, H. S.; Choi, J. A.; Kim, B. Y.; et al. Engineered Corynebacterium glutamicum as the platform for the production of aromatic aldehydes. *Front. Bioeng. Biotechnol.* **2022**, *10*, 880277.
(15) Vignali, E.; Pollegioni, L.; Di Nardo, G.; et al. Multi-enzymatic cascade reactions for the synthesis of cis,cis-muconic acid. *Adv. Synth. Catal.* **2022**, *364*, 114.
(16) https://reports.valuates.com/market-reports/QYRE-Auto-27S9375/global-d-alanine (accessed Jan 12, 2025).
(17) https://reports.valuates.com/market-reports/QYRE-Auto-529/global-l-alanine (accessed Jan 12, 2025).
(18) Li, J.; Yu, S.; Wang, Y.; Yao, P.; Wu, Q.; Zhu, D. Simultaneous preparation of (S)-2-aminobutane and D-alanine or D-homoalanine via biocatalytic transamination at high substrate concentration. *Org. Process Res. Dev.* **2022**, *26*, 2013−2020.
(19) Liu, P.; Xu, H.; Zhang, X. Metabolic engineering of microorganisms for L-alanine production. *J. Ind. Microbiol. Biotechnol.* **2022**, *49*, kuab057.
(20) Tian, S.; Zhao, G.; Lv, G.; et al. Efficient Fermentative Production of D-alanine and other D-amino acids by metabolically engineered. Corynebacterium glutamicum. *J. Agric. Food Chem.* **2024**, *72*, 8039−8051.
(21) Naeem, M.; Hao, S.; Chu, M.; Zhang, X.; Huang, X.; Wang, J.; He, G.; Zhao, B.; Ju, J. Efficient biosynthesis of D/L-alanine in the recombinant Escherichia coli BL21(DE3) by biobrick approach. *Front. Bioeng. Biotechnol.* **2024**, *12*, 1421167.
(22) Rosini, E.; Antonelli, N.; Molla, G. Rethinking plastic waste: innovations in enzymatic breakdown of oil-based polyesters and bioplastics. *FEBS Open Bio* **2025**, 2211-5463.70120.
(23) Bååth, J. A.; Borch, K.; Jensen, K.; Brask, J.; Westh, P. Comparative biochemistry of four polyester (PET) hydrolases. *Chembiochem* **2021**, *22*, 1627−1637.
(24) Arnal, G.; Anglade, J.; Gavalda, S.; et al. Assessment of four engineered PET degrading enzymes considering large-scale industrial applications. *ACS Catal.* **2023**, *13*, 13156−13166.
(25) Palm, G. J.; Reisky, L.; Böttcher, D.; Müller, H.; Michels, E. A. P.; Walczak, M. C.; Berndt, L.; Weiss, M. S.; Bornscheuer, U. T.; Weber, G. Structure of the plastic-degrading Ideonella sakaiensis MHETase bound to a substrate. *Nat. Commun.* **2019**, *10*, 1717.
(26) Fecker, T.; Galaz-Davison, P.; Engelberger, F.; et al. Active site flexibility as a hallmark for efficient PET degradation by I. sakaiensis PETase. *Biophys. J.* **2018**, *114*, 1302−1312.
(27) Cui, L.; Qiu, Y.; Liang, Y.; Du, C.; Dong, W.; Cheng, C.; He, B. Excretory expression of IsPETase in E. coli by an enhancer of signal peptides and enhanced PET hydrolysis. *Int. J. Biol. Macromol.* **2021**, *188*, 568−575.
(28) Shi, L.; Liu, H.; Gao, S.; Weng, Y.; Zhu, L. Enhanced extracellular production of IsPETase in Escherichia coli via engineering of the pelB signal peptide. *J. Agric. Food Chem.* **2021**, *69*, 2245−2252.
(29) Valenzuela-Ortega, M.; Suitor, J. T.; White, M. F. M.; Hinchcliffe, T.; Wallace, S. Microbial upcycling of waste PET to adipic acid. *ACS Cent. Sci.* **2023**, *9*, 2057−2063.
(30) Bao, T.; Qian, Y.; Xin, Y.; Collins, J. J.; Lu, T. Engineering microbial division of labor for plastic upcycling. *Nat. Commun.* **2023**, *14*, 5712.
(31) Barry, K. P.; Taylor, E. A. Characterizing the promiscuity of LigAB, a lignin catabolite degrading extradiol dioxygenase from Sphingomonas paucimobilis SYK-6. *Biochemistry* **2013**, *52*, 6724−6736.
(32) Johnson, C. W.; Salvachua, D.; Rorrer, N. A.; et al. Innovative chemicals and materials from bacterial aromatic catabolic pathways. *Joule* **2019**, *3*, 1523−1537.
(33) Hogancamp, T. N.; Raushel, F. M. Functional annotation of LigU as a 1,3-allylic isomerase during the degradation of lignin in the protocatechuate 4,5-cleavage pathway from the soil bacterium Sphingobium sp. SYK-6. *Biochemistry* **2018**, *57*, 2837−2845.
(34) Wiley, R. H.; Kim, K. S. Bimolecular decarboxylative self-condensation of oxaloacetic acid to citrolyformic acid and its conversion by oxidative decarboxylation to citric acid. *J. Org. Chem.* **1973**, *38*, 3582−3585.
(35) Lerchner, A.; Jarasch, A.; Skerra, A. Engineering of alanine dehydrogenase from Bacillus subtilis for novel cofactor specificity. *Biotechnol. Appl. Biochem.* **2016**, *63*, 616−624.
(36) Tournier, V.; Topham, C. M.; Gilles, A.; et al. An engineered PET depolymerase to break down and recycle plastic bottles. *Nature* **2020**, *580*, 216−219.
(37) Johnson, C. W.; Beckham, G. T. Aromatic catabolic pathway selection for optimal production of pyruvate and lactate from lignin. *Metab. Eng.* **2015**, *28*, 240−247.
(38) Tiso, T.; Narancic, T.; Wei, R.; et al. Towards bio-upcycling of polyethylene terephthalate. *Metab. Eng.* **2021**, *66*, 167−178.
(39) Werner, A. Z.; Avina, Y. C.; Johnsen, J.; et al. Adaptive laboratory evolution and genetic engineering improved terephthalate utilization in Pseudomonas putida KT2440. *Metab. Eng.* **2025**, *88*, 196−205.
(40) Umdagas, L.; Orozco, R.; Heeley, K.; Thom, W.; Al-Duri, B. Advances in chemical recycling of polyethylene terephthalate (PET) via hydrolysis: a comprehensive review. *Polym. Degrad. Stab.* **2025**, *234*, 111246.
(41) https://reports.valuates.com/ (accessed July 12, 2025).
(42) https://www.researchandmarkets.com/ (accessed July 12, 2025).
(43) Pirillo, V.; Pollegioni, L.; Molla, G. Analytical methods for the investigation of enzyme-catalyzed degradation of polyethylene terephthalate. *FEBS J.* **2021**, *288*, 4730−4745.
(44) Saran, M.; Summer, K. H. Assaying for hydroxyl radicals: hydroxylated terephthalate is a superior fluorescence marker than hydroxylated benzoate. *Free Radic. Res.* **1999**, *31*, 429−436.

https://doi.org/10.1021/acscatal.5c06530
ACS Catal. 2025, 15, 17829−17843